ELSEVIER International Journal of Mass Spectrometry and Ion Processes 153 (1996) 65–78

International Journal of Mass Spectrometry and Ion Processes

Electron impact ionization of tetramethylsilane (TMS)

R. Basner, R. Foest, M. Schmidt*, F. Sigeneger, P. Kurunczi[1], K. Becker[1], H. Deutsch[2]

Institut für Niedertemperatur-Plasmaphysik (INP), Greifswald, Germany

Received 30 October 1995; accepted in final form 7 December 1995

Abstract

We studied the electron impact ionization of tetramethylsilane (TMS), $Si(CH_3)_4$, which is utilized in plasma polymerization applications, using various mass spectrometric techniques. Absolute partial cross-sections for the formation of the parent ion and 15 fragment ions were measured in a high resolution double-focusing sector field mass spectrometer from threshold to 90 eV. Complementary measurements of mass spectral cracking patterns of TMS were also carried out using two quadrupole mass spectrometers. Dissociative ionization of TMS was found to be the dominant process. The $Si(CH_3)_3^+$ ion is by far the most abundant fragment ion with a maximum cross-section of about 1×10^{-15} cm^2. In contrast, the maximum parent ionization cross-section is less than 2% of that value. On the basis of the measured partial ionization cross-sections, mass spectral cracking patterns and appearance energies of the various ionic products, we propose a collision-induced decomposition scheme for the TMS molecule. Three major decomposition channels were identified which all involve the total or partial removal of a methyl group. The agreement of our measured absolute partial ionization cross-sections with earlier data obtained by a different technique is generally poor.

Keywords: Cross-sections; Electron impact ionization; Plasma deposition

1. Introduction

Low temperature plasma technology is a rapidly growing field which plays a key role in many high tech applications such as plasma-assisted thin film deposition, plasma etching, and surface treatment and cleaning. The plasma-assisted polymerization is one of the most widely used thin film deposition techniques for surface protection and surface modification of optical devices, electronics components and in biomedical applications [1]. Hydrocarbons, organometallic and organosilicon compounds are commonly used monomers for these purposes. Organosilicon compounds are of particular interest for many deposition applications due to the superior properties of their polymers. The most widely used compounds include hexamethyldisiloxane [2], tetraethoxysilane [3,4], hexamethyldisilazane [5], and tetramethylsilane (TMS) [6,7] which is the simplest organosilicon compound. TMS, $Si(CH_3)_4$, is a precursor in the plasma-assisted chemical vapor deposition (PACVD) of SiN and SiC films [8] and it is

* Corresponding author.

[1] Permanent address: Physics Department, City College of C.U.N.Y., New York, USA.

[2] Permanent address: Fachbereich Physik, E.M.A. Universität Greifswald, Germany.

SSDI 0168-1176(95)04352-7

also an abundant reaction product in processing plasmas containing more complex organosilicon monomers [9,10]. The electron impact ionization of the monomer is one of the most fundamental collision processes in a non-equilibrium, low temperature plasma used in plasma polymerization applications. The detailed understanding and modeling of the plasma-enhanced deposition process require a knowledge of the total and partial electron impact ionization cross-sections. The shape of the cross-section in the low energy near-threshold region is particularly important for the properties of a low temperature plasma, since this is the energy regime of maximum overlap between the ionization cross-section and the energy distribution function of the plasma electrons [11]. Electron impact induced ionization is not only the dominant process for the formation of charge carriers in the plasma, it is also the crucial step that initiates the multitude of plasma chemical reactions through the formation of reactive neutral and ionic radicals via dissociative ionization of the often inert feed-gas molecules [11,12].

Electron impact ionization cross-sections of tetramethylsilane have been measured previously by McGinnis et al. [13] using Fourier transform mass spectrometry. In addition, ionization and appearance energies were measured in previous electron impact and photo-ionization experiments (see Refs. [14] and [15] and references cited therein). The mass spectrum of TMS at 70 eV is also contained in standard mass spectrometric data bases (see for example Ref. [16]). Optical emissions from the vacuum ultraviolet to the visible region of the spectrum resulting from the single electron impact on TMS and other organosilicon compounds have recently been analyzed by Becker and co-workers [17,18].

This paper presents the results of the mass spectrometric measurement of absolute partial and total electron impact ionization cross-sections of TMS. Most measurements were carried out in a high resolution double-focusing sector field mass spectrometer. These studies were complemented by a series of measurements of mass spectral cracking patterns involving the use of two quadrupole mass spectrometers, primarily for the benefit of plasma practitioners who often use such instruments for plasma monitoring and plasma diagnostics purposes. A collision-induced decomposition scheme for the TMS molecule, which is also relevant for decomposition in low temperature plasmas is proposed and will be discussed in connection with similar data for the tetramethyl compounds of the elements C, Ge, Sn, and Pb, which are in the same group as Si in the periodic system. The experimentally determined total (single) TMS ionization cross-section is compared to the results of several semiempirical calculations. The results obtained in this work are important for a better understanding and an improved modeling of TMS-containing low temperature processing plasmas and of plasmas featuring more complex organosilicon molecules in which TMS is a major reaction product.

2. Experimental details

Most of the measurements were carried out in a high resolution ($m/\Delta m = 40\,000$) double-focusing sector field mass spectrometer (MCH 1310) of the E–H configuration with a Nier-type electron impact ion source. Full details of the apparatus and of the experimental procedure have been described in previous publications [19,20]. Briefly, the ion source was operated at a gas pressure in the range 0.1–1 mPa as measured by a spinning rotor viscosity gauge. TMS, a liquid at room temperature, was placed in a reservoir which is connected to the ionization chamber via a UHV high precision leak valve. The TMS vapor pressure at room temperature is

sufficiently high to produce a target gas pressure in the interaction region in the millipascal regime. The temperature of the ion source was kept at 100°C. Argon was always added as a reference gas for energy calibration and normalization purposes and ionization efficiency curves were recorded simultaneously for both Ar and TMS. The electron gun was operated with a stabilized electron beam current of 10 μA emitted by a directly heated tungsten band cathode. The impact energy could be varied between close to 0 eV and about 90 eV. The energy spread of the electron beam, which is collimated by a weak longitudinal magnetic field of 200 G, was about 0.5 eV (FWHM). Ions were extracted from the ionization region by a penetrating electric field. The acceleration voltage between the ion source and the entrance slit of the mass spectrometer was 5 kV. The ion repeller potential was kept at the potential of the ionization chamber.

The reliability of the mass spectrometric technique for the absolute measurement of parent ionization cross-sections and, more recently, also for fragment ionization cross-sections was demonstrated by Märk and co-workers [21–23]. These authors pointed out that discrimination effects and the loss of energetic fragment ions must be accounted for in order to obtain reliable dissociative ionization cross-sections. Earlier measurements of the NF_3 parent and fragment ionization cross-sections in our apparatus [24] revealed a significant loss of energetic fragment ions. As a consequence, the ion optical system for the extraction and acceleration of the ions was rebuilt based on ion trajectory simulations [25] in conjunction with in situ experimental studies in an effort to minimize and/or to quantify the discrimination of energetic fragment ions. The modified mass spectrometer can now be operated either in a high mass resolution mode (with significant discrimination effects present) or in a high extraction efficiency mode (by partially sacrificing the high mass resolution capability). Recent ionization cross-section measurements for SO_2 [19] carried out in our modified mass spectrometer as well as in a fast-neutral beam apparatus, which is less sensitive to discrimination effects, revealed that the mass spectrometer operated in the high extraction efficiency mode can detect energetic fragment ions with a significantly higher efficiency than in the high mass resolution mode as long as the excess kinetic energy is sufficiently small (e.g. less than about 1 eV per fragment in the case of SO^+, S^+ and O^+ from SO_2 [19]).

The measured relative partial ionization cross-sections were put on an absolute scale by normalization relative to the total ionization cross-sections of 2.77×10^{-16} cm^2 at 70 eV for Ar [26] which is used as reference gas in a well-defined mixture with the target gas under study [20]. The total TMS ionization cross-section, which is identical to the total single ionization cross-section due to the dominance of the single ionization channels (see below), was obtained as the sum of the measured partial ionization cross-sections. The combined statistical and systematic uncertainty in the absolute ionization cross-sections reported here is about ±20% [20,24]. Appearance energies were determined by calibrating the electron energy scale relative to the ionization energies of the rare gases Ar, Kr and Xe and could be measured with an uncertainty of typically ±0.5 eV. Larger uncertainties are possible in cases where the ion signals were very low or where the ionization cross-section exhibited an extended curvature in the near-threshold region. This extended curvature may be caused by the several different ionization channels with different appearance energies contributing to the recorded ion signal at a given mass-per-charge (m/z) ratio (see below).

Complementary measurements of the mass spectral cracking patterns of TMS were carried out using two quadrupole mass spectrometers,

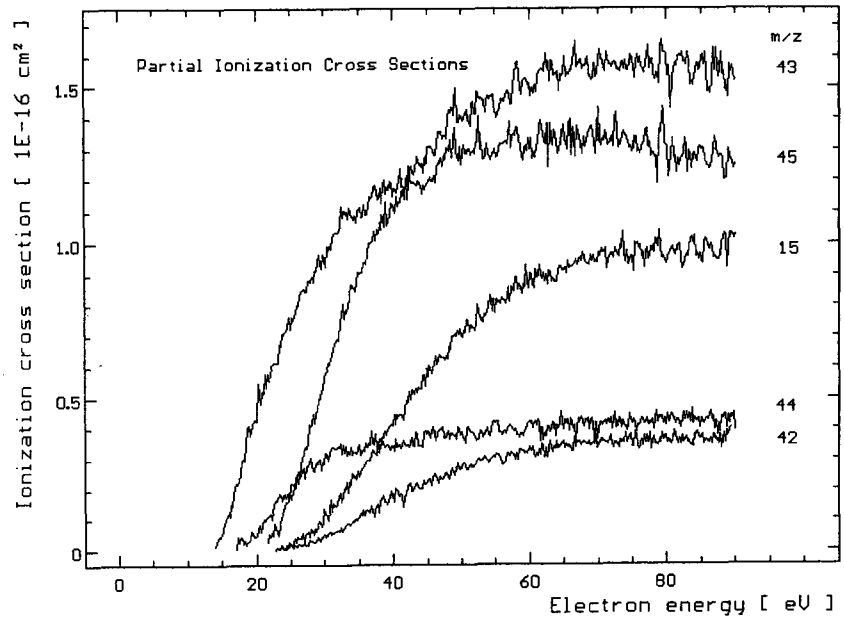

Fig. 1. Partial ionization cross-sections of the TMS fragment ions CH_3^+ (m/z 15), $SiCH_2^+$ (m/z 42), $SiCH_3^+$ (m/z 43), $HSiCH_3^+$ (m/z 44) and $H_2SiCH_3^+$ (m/z 45), obtained with MCH1310.

a VG model SXP 300H which is also equipped with a cylindrical mirror analyzer (CMA) for ion energy analysis and a Balzers model QMG 421. Both instruments have a comparatively "open" ion source which leads to a much reduced discrimination of energetic ions as far as the ion extraction is concerned. On the other hand, both instruments have an

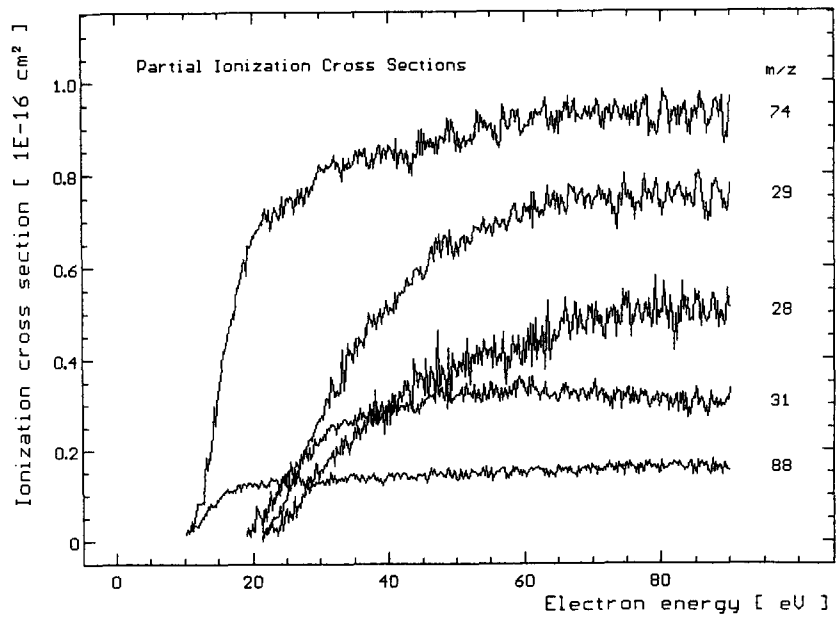

Fig. 2. Partial ionization cross-sections of the TMS parent molecule (m/z 88) and the fragment ions Si^+ (m/z 28), HSi^+ (m/z 29), H_3Si^+ (m/z 31), and $HSi(CH_3)_3^+$ (m/z 74), obtained with MCH1310.

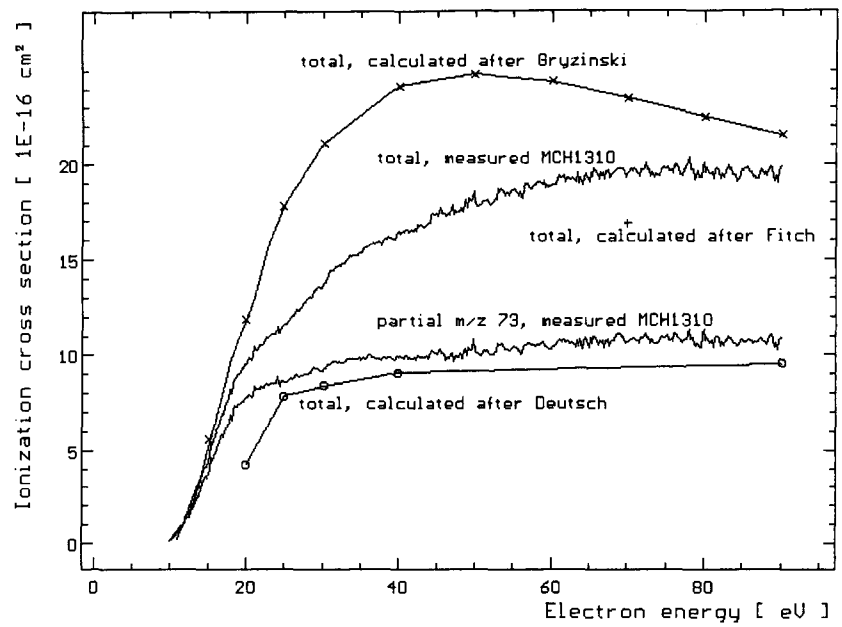

Fig. 3. Partial ionization cross-section of the TMS fragment ion $Si(CH_3)_3^+$ (m/z 73) and total ionization cross-section of the TMS molecule, obtained with MCH1310, in comparison with calculated total cross-sections after Gryzinski (×) [38], Fitch and Sauter (+, at 70 eV) [30] and Deutsch et al. (O) [29].

extended ionization region and a mass-dependent transmission of the quadrupole field which renders absolute ionization cross-section measurements difficult, if not impossible, using these quadrupole mass spectrometers.

3. Results and discussion

Selected results of the ionization cross-section measurements for TMS are presented in Figs. 1–3. Figs. 1 and 2 show the cross-sections for formation of the fragment ions corresponding to m/z values of 15 (CH_3^+), 28 (Si^+), 29 (SiH^+), 31 (SiH_3^+), 42 ($SiCH_2^+$), 43 ($SiCH_3^+$), 44 ($HSiCH_3^+$), 45 ($H_2SiCH_3^+$ and 74 ($HSi(CH_3)_3^+$) as well as the parent ionization cross-section (molecular peak, m/z 88) from threshold to about 90 eV. The respective m/z values are indicated on the right-hand side of each cross-section curve. We note that in some cases the recorded ion signals contain a mixture of ions with different Si isotopes and ions of a different chemical composition, e.g. the signal at m/z 29 consists of $^{28}SiH^+$ ions and $^{29}Si^+$ ions. Since natural Si is dominated by the isotope ^{28}Si (92.3% abundance) and the other isotopes are much less abundant, ^{29}Si (4.7%) and ^{30}Si (3.0%), this contamination of the recorded ion signals is small compared to the overall uncertainty of the measured absolute ionization cross-sections, but may result in an extended curvature in the near-threshold region of the cross-section. Maximum cross-sections of close to 1.5×10^{-16} cm^2 were found for the ion signals at m/z values of 43 and 45. The maximum cross-section for the methyl ion (m/z 15) reaches a value of about 1×10^{-16} cm^2 at about 80 eV. All other maximum cross-section values shown in Figs. 1 and 2 are below 1×10^{-16} cm^2. We note that the measured CH_3^+ cross-section represents a lower limit, since these fragment ions are formed with a wide distribution of excess

Table 1
Partial and total cross-section values for electron impact ionization of TMS

Electron energy (eV)	Partial ionization-cross section (10^{-16} cm^2)															
	m/z															
	15	28	29	31	42	43	44	45	53	55	57	58	59	73	74	88	Total
10														0.160		0.004	0.164
11														0.585	0.045	0.027	0.657
12														1.376	0.083	0.034	1.493
13														1.778	0.135	0.061	1.974
14								0.014						3.023	0.217	0.078	3.332
15								0.052						3.828	0.327	0.088	4.295
16								0.117					0.009	4.824	0.415	0.103	5.468
17								0.203					0.021	5.735	0.477	0.109	6.545
18								0.295			0.005	0.005	0.039	6.573	0.557	0.119	7.593
19				0.015				0.409			0.017	0.007	0.059	7.465	0.600	0.123	8.695
20				0.036				0.422			0.021	0.010	0.071	7.779	0.607	0.125	9.071
21				0.054		0.021	0.093	0.517		0.003	0.036	0.015	0.087	8.177	0.686	0.127	9.816
22		0.019	0.031	0.061		0.043	0.115	0.577		0.007	0.042	0.019	0.123	8.337	0.703	0.129	10.206
23		0.022	0.052	0.090	0.005	0.061	0.170	0.614		0.010	0.052	0.023	0.138	8.498	0.712	0.130	10.577
24	0.012	0.030	0.059	0.117	0.009	0.130	0.173	0.703		0.015	0.058	0.033	0.151	8.562	0.720	0.130	10.902
25	0.023	0.054	0.098	0.141	0.013	0.181	0.213	0.746	0.004	0.025	0.070	0.036	0.166	8.658	0.737	0.132	11.297
26	0.040	0.065	0.135	0.155	0.014	0.246	0.228	0.800	0.009	0.048	0.079	0.045	0.173	8.786	0.740	0.133	11.696
27	0.046	0.095	0.179	0.183	0.019	0.321	0.262	0.856	0.012	0.066	0.088	0.053	0.175	8.914	0.748	0.134	12.151
28	0.058	0.115	0.216	0.198	0.027	0.411	0.274	0.876	0.012	0.072	0.096	0.061	0.185	9.043	0.754	0.135	12.533
29	0.079	0.120	0.220	0.198	0.035	0.426	0.285	0.900	0.012	0.090	0.102	0.068	0.201	9.139	0.774	0.135	12.784
30	0.138	0.149	0.267	0.222	0.048	0.569	0.285	0.956	0.016	0.095	0.110	0.072	0.201	9.235	0.808	0.135	13.306
32	0.163	0.187	0.321	0.253	0.067	0.687	0.337	1.037	0.030	0.140	0.119	0.096	0.215	9.555	0.820	0.135	14.162
34	0.235	0.214	0.404	0.259	0.097	0.859	0.323	1.084	0.045	0.169	0.120	0.111	0.214	9.812	0.820	0.136	14.902
36	0.238	0.245	0.432	0.273	0.124	0.931	0.343	1.090	0.055	0.188	0.120	0.122	0.215	9.844	0.837	0.139	15.196
38	0.285	0.253	0.453	0.276	0.128	0.939	0.348	1.093	0.060	0.190	0.120	0.126	0.220	9.844	0.842	0.139	15.316
40	0.445	0.285	0.528	0.291	0.193	1.129	0.361	1.173	0.099	0.222	0.122	0.153	0.228	9.943	0.845	0.140	16.157
45	0.580	0.351	0.587	0.305	0.221	1.295	0.378	1.190	0.147	0.256	0.131	0.185	0.233	10.036	0.865	0.143	16.903
50	0.706	0.383	0.642	0.321	0.274	1.403	0.383	1.281	0.181	0.261	0.131	0.211	0.234	10.164	0.976	0.144	17.695
55	0.802	0.412	0.679	0.325	0.303	1.446	0.396	1.289	0.203	0.273	0.132	0.230	0.243	10.324	0.893	0.148	18.098
60	0.880	0.424	0.716	0.333	0.325	1.495	0.400	1.304	0.236	0.279	0.134	0.243	0.247	10.389	0.913	0.149	18.467
70	0.958	0.487	0.744	0.328	0.349	1.574	0.410	1.330	0.266	0.281	0.134	0.248	0.250	10.741	0.930	0.158	19.188
80	0.967	0.518	0.744	0.316	0.370	1.574	0.422	1.332	0.282	0.282	0.136	0.246	0.256	10.805	0.925	0.160	19.335
90	1.000	0.518	0.746	0.316	0.390	1.578	0.422	1.332	0.295	0.285	0.139	0.248	0.256	10.805	0.913	0.160	19.403

Table 2
Normalized peak intensities of the TMS mass spectrum at 70 eV impact energy obtained in this work using the three different mass spectrometers MCH 1310, Balzers QMG 421 and VG SXP 300H. Also listed are relative intensities taken from the literature (Eight Peak Index (Data Base) [16] and McGinnis et al. (FTMS) [13])

m/z	Data base	MCH 1310	QMG 421	SXP 300H	FTMS
2			9.7	1.0	
15	6	8.9	4.5	3.0	
27				1.4	
28		4.5	4.6	6.1	
29	7	6.9	5.1	10.2	
31		3.3	3.2	6.3	
42	4	3.2		6.4	
43	16	14.6	10.2	27.9	11.0
44	5	3.9	3.2	8.8	
45	13	12.0	14.0	39.0	20.1
53		2.4		4.6	
55		2.7	1.4	4.2	
57		1.2	1.0	2.6	
58		2.3	0.9	2.7	
59		2.3	1.3	3.0	
73	100	100	100	100	100
74	8	9.7	5.5	9.1	
88		1.5	0.9	0.8	4.2

kinetic energies (see discussion below) and thus the quantitative detection of CH_3^+ fragment ions is likely to be affected by discrimination effects (see earlier discussion). It is noteworthy that the parent ionization cross-section (*m/z* 88) is very small with a peak value of 0.16×10^{-16} cm^2. This finding is very similar to what was observed before in ionization studies of several complex organometallic compounds [20]. By far the largest ionization cross-section with a peak value of almost 11×10^{-16} cm^2 was measured for *m/z* 73 (base peak) which corresponds to the $Si(CH_3)_3^+$ fragment ion. This cross-section is shown in Fig. 3 together with the total TMS ionization cross-section and the results of several semiempirical cross-section calculations (which will be discussed later). The values of all 16 ionization cross-sections measured in this work are summarized in tabulated form for easier quantitative reference in Table 1. Also given are numerical values for the total TMS ionization cross-section.

Table 2 summarizes the measured cracking patterns of the TMS molecule (at an impact energy of 70 eV) obtained in this work using the three different mass spectrometers (MCH 1310, QMG 421, and SXP 300H). Also listed is the cracking pattern from the Eight Peak Index [16] and the cracking pattern obtained by McGinnis et al. [13] using Fourier transform mass spectrometry (FTMS). We note that the cracking patterns measured in the MCH 1310 in the high extraction efficiency mode and in the high resolution mode were nearly identical which indicates that most fragment ions are formed with little excess kinetic energy. The only exception to this is the peak at *m/z* 15 corresponding to the methyl ion, CH_3^+, where the peak height obtained in the high extraction mode was three times higher than the peak height measured in the high resolution mode. This observation prompted us to measure the energy distribution of CH_3^+ ion formed by dissociative ionization of TMS using the CMA of the SXP 300H mass spectrometer. Fig. 4 shows the fragment energy distribution measured for the CH_3^+ ions

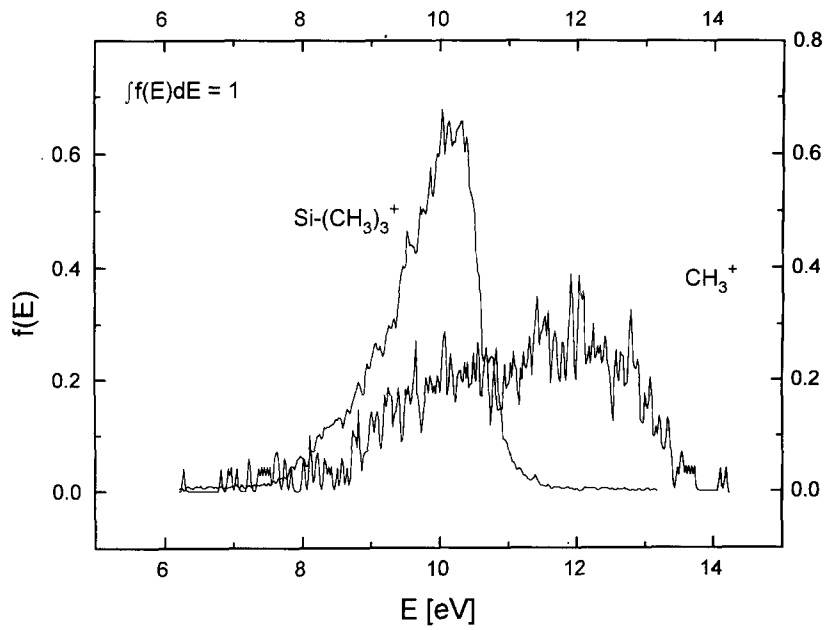

Fig. 4. Normalized energy distribution of the $Si(CH_3)_3^+$ and CH_3^+ ions, measured with the cylindrical mirror analyzer (CMA) of the SXP 300H with a 10 eV acceleration energy between ion source and the CMA (see text for further details).

in comparison with the energy distribution of the $Si(CH_3)_3^+$ ions (*m/z* 73). The energy distribution of the $Si(CH_3)_3^+$ ions is representative for all observed ions except for CH_3^+. The acceleration energy between the ion source and the CMA was 10 eV during the measurements. The $Si(CH_3)_3^+$ fragment ions show a narrow energy distribution centered at 10 eV with a width (FWHM) of about ±0.5 eV which reflects the energy resolution of the CMA. This indicates that the $Si(CH_3)_3^+$ fragment ions, as most other fragment ions, are near thermal with an excess kinetic energy which is small compared to the ±0.5 eV energy resolution of the CMA. The CH_3^+ ions, on the other hand, exhibit a broad energy distribution whose maximum is shifted by about 2 eV toward higher energies indicating that these ions are formed with a wide distribution of excess energies peaking at about 2 eV.

All TMS cracking patterns listed in Table 2 are normalized to the base peak at *m/z* 73 which is the strongest signal in all TMS mass spectra. The molecular ion signal ($M^{\cdot+}$) (*m/z* 88) was found to be small in all cases (about 1% of the base peak), although there is a difference in its intensity of a factor of 2 between the three different instruments used in this work. The $M^{\cdot+}$ ion signal obtained from the FTMS data is larger than any of our measurements (about 4% of the base peak). Other significant fragment ions are those at *m/z* 45 and 43. Their intensities are similar at roughly 15% of the base peak (as measured with the MCH 1310 and the QMG 421). This finding is in agreement with the data in the known data base [16] and with the FTMS data [13]. We note that the mass spectra obtained with the SXP 300H show consistently higher intensities in the *m/z* range from the base peak (*m/z* 73) down to *m/z* 28 which we attribute to a higher sensitivity of this particular mass analyzer in this mass range. It is not surprising that the methyl ion peak at *m/z* 15 is largest in the MCH 1310 mass spectrum (obtained in the high extraction efficiency mode), since these fragment ions are formed

Table 3
Systematics of the detected ions for TMS with their measured appearance energies (E_a)

H loss by CH_3 decay			Complete methyl groups			H transfer from CH_3 groups		
m/z	Ion	E_a (eV)	m/z	Ion	E_a (eV)	m/z	Ion	E_a (eV)
			88	$Si(CH_3)_4^+$	9.9			
						74	$HSi(CH_3)_3^+$	10.4
			73	$Si(CH_3)_3^+$	10.1			
						59	$HSi(CH_3)_2^+$	15.6
			58	$Si(CH_3)_2^+$	17.6			
57	$SiC_2H_5^+$	17.6						
55	$SiC_2H_3^+$	20.8						
53	SiC_2H^+	25.1						
						45	$H_2Si(CH_3)^+$	13.8
						44	$HSi(CH_3)^+$	17.2
			43	$Si(CH_3)^+$	20.1			
42	$SiCH_2^+$	22.7						
						31	H_3Si^+	18.9
						29	HSi^+	21.2
			28	Si^+	21.2			
			15	CH_3^+	23.4			
2	H_2^+							
1	H^+							

with a certain amount of excess kinetic energy (see above). None of the instruments used in the present studies (or in any of the previous studies) was capable of determining reliable intensities of the atomic hydrogen ions.

A proposed collision-induced decomposition scheme for the TMS molecule, which is also relevant in low temperature plasmas, is given in Table 3 which summarizes the detected ions together with their measured appearance energies. Ionization and appearance energies for the TMS parent ion and for the various fragment ions are known from literature for m/z 88 (9.74 eV [15], 9.69 eV and 9.86 eV [15]), m/z 73 (10.25 eV [14], 9.90 eV, and 10.09 eV [15]) and m/z 45 (13.6 eV and 13.81 eV [15]). The appearance energies measured in this work are in good agreement with these values within the stated uncertainty of ± 0.5 eV (see also Tables 3 and 4 below). The corresponding FTMS values obtained by McGinnis et al. [13] are different from these values which might be attributed to the fact that their appearance energies are derived from a mathematically more involved data reduction procedure.

The formation of the Si-containing fragment ions proceeds via three different mechanisms:

(i) the removal of a complete methyl group;

(ii) the removal of a complete methyl group and an additional hydrogen atom (perhaps leading to the formation of the stable CH_4 (methane) molecule);

(iii) the removal of a CH_2 or CH group with one or two H atoms remaining with the ion (this process is most likely followed by a rearrangement of the remaining H atoms within the residual ion).

The appearance energy of an ion formed via process (ii) is generally higher than that of an ion formed via process (i). Ions formed via process (iii) require less energy than ions formed via process (i) with the exception of the $HSi(CH_3)_3^+$ ion. A possible explanation for this might be the remarkably small energy difference between the ionization energy of the parent ion (9.9 eV) and the 10.1 eV appearance

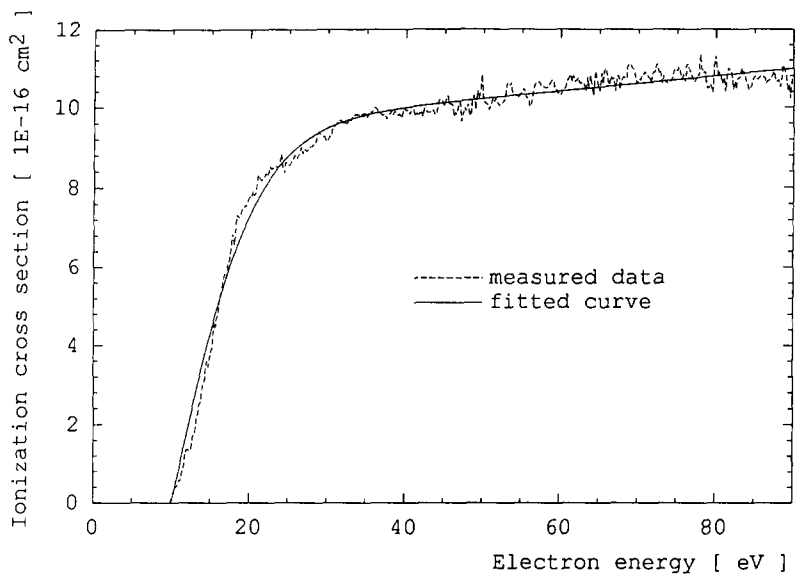

Fig. 5. Measured partial ionization cross-section of the TMS fragment ion $Si(CH_3)_3^+$ (m/z 73) together with the fitted curve, using Eq. (1), showing a very good fit for the whole energy range.

energy of the most abundant fragment ion $Si(CH_3)_3^+$. Since the average Si–C bond energy is about 3.2 eV [27], the 0.2 eV difference in the appearance energies for the two ions is most likely due to a lower energy of the planar $Si(CH_3)_3^+$ ion in comparison to the tetragonal $Si(CH_3)_4^+$ ion. This effect was discussed by McGinnis et al. [13] on the basis of the Jahn–Teller theorem in connection with the low intensity of the parent ion.

It is interesting to compare the mass spectral cracking patterns of TMS with those of the tetramethyl compounds of other elements in the same group of the periodic table (C, Ge, Sn and Pb). The only data available for comparison are those listed in the standard mass spectroscopic data base [16]. All mass spectra show qualitatively similar patterns, particularly those of the lighter elements. In all cases, the $M^{\cdot+}$ signal is very small and the most intense signal (base peak) is due to the removal of one methyl group. The subsequent removal of additional CH_3 groups results in peaks of lower intensity. In the case of Ge, the GeH^+ peak is more intense than the Ge^+ peak. For both C and Ge, the $CH_3XH_2^+$ (X=C,Ge) intensities are larger than the CH_3X^+ peaks which is similar to what we found for the Si compound.

A detailed comparison of our TMS ionization cross-sections with the values reported by McGinnis et al. [13] reveals good agreement in terms of the cross-section shapes reported by both groups, but poor agreement in terms of the absolute cross-section values for some of the most intense ion peaks. Our measured cross-sections are distinctly higher by about a factor of 2 for the most abundant $Si(CH_3)_3^+$ fragment ion and for the ion signal at m/z 43 and slightly higher for the peak at m/z 45. While McGinnis et al. [13] report ionization cross-sections in the 10^{-18} cm^2 range (at 70 eV) for m/z 53, 55, 57, 58 and 59, we measured values in the 10^{-17} cm^2 range for these ions (see Table 1). McGinnis et al. [13] did not report cross-sections for the formation of ions with m/z <43, whereas we observed several prominent ion signals for m/z values between 43 and 15.

McGinnis et al. [13] give a simple fitting

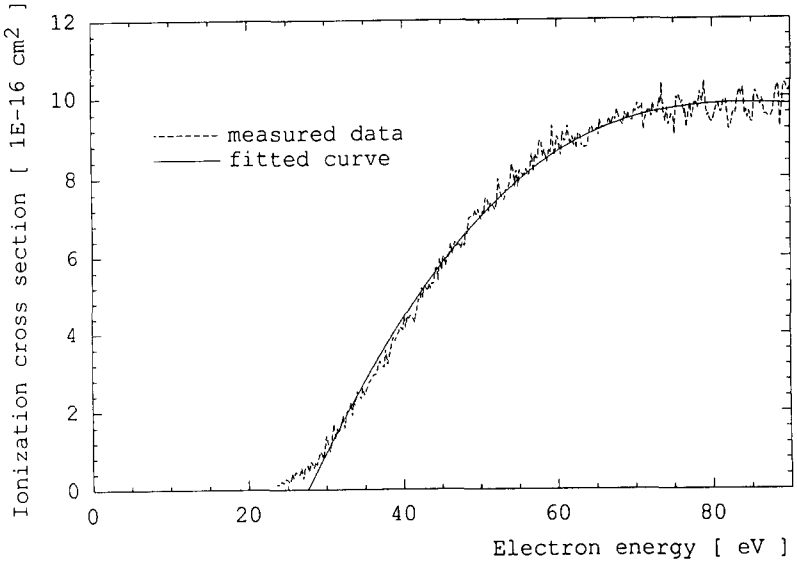

Fig. 6. Measured partial ionization cross-section of the TMS fragment ion CH_3^+ (m/z 15) together with the fitted curve, using Eq. (1). The extended curvature in the near-threshold region is not adequately described by the fitting formula.

formula for the analytical representation of ionization cross-sections for modeling purposes:

$$\sigma(\epsilon) = A\exp[(-k)(\epsilon - T)]\tanh[\pi(\epsilon - T)/\alpha] \quad (1)$$

where σ is the ionization cross-section, ϵ is the electron energy, T is the appearance energy, A is a scaling parameter determined by the maximum in the cross-section, k determines the shape of the cross-section curve at higher electron energies, and α is related to cross-section slope in the near-threshold region. We applied this fitting formula to our cross-sections in an effort to facilitate a more convenient use of our data for modeling purposes. The fitting parameters have been obtained by using the Levenberg–Marquard method [28]. In many cases, the fitting formula provides a very good representation of the measured cross-section over the entire energy range as shown in Fig. 5 for the $Si(CH_3)_3^+$ cross-section. However, cross-section curves with an extended curvature in the near-threshold region could not be represented adequately by this formula at very low energies (see for example Fig. 6). Table 4 summarizes the fitting parameters for the ionization cross-sections measured in this work together with the fitting parameters derived by McGinnis et al. [13]. Also shown in Table 4 are the experimentally determined appearance energies. A significant difference between the experimentally determined appearance energy U_{exp} and the fitting parameter T indicates a cross-section curve displaying extended curvature in the near-threshold region. The near-threshold region of a cross-section with extended curvature should not be approximated by the above fitting formula for modeling purposes. The correct shape of the ionization cross-section in the near-threshold region, where the electron energy distribution function of the plasma electron varies rapidly as a function of energy, is a crucial input parameter for reliable modeling and simulations. We also applied the above fitting formula to the total single TMS ionization cross-section.

The total single TMS ionization cross-section, which is shown in Fig. 3 and listed in

Table 4
Fitting parameters for the representation of the measured partial and total cross-section curves from Eq. (1). Also listed are the values taken from McGinnis et al. [13] for comparison, along with experimentally determined appearance energies U_{exp} (see text for further details)

m/z	$A \times 10^{16}$ (cm^{-2})	[13]	$k \times 10^{3}$ (eV^{-1})	[13]	α (eV)	[13]	T (eV)	[13]	U_{exp} (eV)
15	1.40		4.69		112		27.6		23.4
28	0.403		−3.81		68.5		21.8		21.2
29	0.784		0.537		71.2		21.8		21.2
31	0.369		2.68		53.3		18.3		18.9
42	0.417		1.77		88.9		27.2		22.7
43	1.66	0.95	0.938	6.26	64.3	61.5	22.7	24.1	20.1
44	0.347		−3.17		33.1		17.9		17.1
45	1.39	1.43	1.03	2.36	58.4	33.1	13.9	15.3	13.8
53	0.346		1.51		114		28.0		25.1
55	0.347		3.74		66.7		22.9		20.8
57	0.127		−1.28		36.0		17.6		17.6
58	0.491		9.15		142		21.8		17.6
59	0.222		−2.07		31.5		16.2		15.6
73	9.41	6.91	−2.01	2.17	27.8	28.7	10.8	18.5	10.1
74	0.797		2.32		27.6		11.1		10.4
88	0.125	0.26	−3.57	0.77	18.3	45.1	9.73	5.4	9.9
Total	17.1	9.18	−1.93	1.33	60	34.2	9.65	12.6	9.9

Table 1, is given as the sum of the measured partial ionization cross-sections for the formation of singly charged ions. We note that no evidence was found that multiply charged TMS parent or fragment ions are formed with appreciable cross-sections. The total single ionization increases rapidly from threshold to 30 eV. Subsequently, the cross-section increases very gradually between 30 eV and the maximum value of about 19×10^{-16} cm^2 which is reached around 80 eV. Our total TMS ionization cross-section is larger than the cross-section reported by McGinnis et al. [13] by roughly a factor of 2 which is the result of the significant differences in some of the partial ionization cross-sections. In the absence of rigorous theoretical methods that can be applied to the calculation of (total) ionization cross-sections for complex molecules, various semiempirical methods are frequently used (see Ref. [29] for a recent summary). Several variants of the additivity rule which expresses the molecular ionization cross-section in terms of the ionization cross-sections of the constituent atoms have been applied to TMS. The additivity rule of Fitch and Sauter [30,31] using a statistical treatment of the atomic ionization cross-sections yields a total TMS ionization cross-section of 16.8×10^{-16} cm^2 at 70 eV which agrees reasonably well with the experimentally determined total ionization cross-section. A modified additivity rule which was recently introduced by Deutsch et al. [29] incorporates weighting factors in an effort to account for molecular bonding. Even though this modified additivity rule has been successfully applied to simple molecules and free radicals [32–34], its application to the TMS molecule using available cross-sections for H [35], C [36] and Si [37] yields a calculated cross-section which underestimates our measured cross-section by roughly a factor of 2. Also shown in Fig. 3 is the calculated total TMS cross-section based on the Gryzinski formula [38] and the data of Daniels et al. [39] for the number of electrons in the various molecular orbitals of TMS and

their respective ionization energies. The calculated cross-section based on the Gryzinski formula overestimates the experimentally determined cross-section, particularly at lower impact energies.

4. Conclusions

We measured absolute partial cross-sections for the electron impact ionization and dissociative ionization of the simplest organosilicon molecule TMS using a mass spectrometric technique. By far the most dominant channel is the formation of the $Si(CH_3)_3^+$ fragment ion with a maximum cross-section of about 1×10^{-15} cm^2. In contrast, the maximum parent ionization cross-section is less than 2% of that value. We propose a collision-induced decomposition scheme for the TMS molecule in low temperature plasmas and identified three major decomposition mechanisms which all involve the total or partial removal of a CH_3 group. In order to facilitate the use of our measured ionization cross-section data we present a set of fitting parameters which can be used to express all measured partial TMS ionization cross-sections as well as the total TMS ionization cross-section in an analytical form. A comparison of our measured cross-section with the ionization cross-section measured earlier using a different technique reveals generally poor agreement. Likewise, the agreement between the experimentally determined and calculated total TMS ionization cross-sections based on various semiempirical methods is less than satisfactory except for the result of one variant of the additivity rule.

Acknowledgments

This work was supported by a NATO Collaborative Research Grant (CRG-920089). We thank Mrs Haeder for invaluable technical assistance. Two of us (P.K. and K.B.) would like to acknowledge partial financial support from the U.S. National Science Foundation (NSF) through grant PHY-9401874. P.K. and K.B. would also like to thank their collaborators in Greifswald for their hospitality and support during several visits.

References

[1] R. d'Agostino (Ed.), Plasma Deposition, Treatment and Etching of Polymers, Academic Press, San Diego, 1990.
[2] H. Yasuda, Plasma Polymerization, Academic Press, London, 1985.
[3] A.W. Luft and S. Tsuo, Appl. Phys. Commun., 8 (1988) 1.
[4] D.A. Gougherty and A. Gallagher, J. Appl. Phys., 67 (1990) 139.
[5] A.M. Wrobel, M. Kryszewski and M. Gazicki, J. Macromol. Sci. Chem. A, 201 (1983) 583.
[6] I. Tajama and M. Yamamoto, J. Polym. Sci.: Part A Polym. Chem., 25 (1987) 1737.
[7] P. Favia, R. Lamendola and R. d'Agostino, Plasma Sources Sci. Technol., 1 (1992) 59.
[8] S. Peter, R. Pintaske, G. Hecht and F. Richter, Surf. Coat. Technol., 59 (1993) 97.
[9] M. Schmidt, R. Foest, R. Basner and M. Hannemann, Acta Phys. Univ. Comenianae, 35 (1994) 217.
[10] R. Jurani, R. Lamendola, R. di'Agostino and J. Trnovec, in P. Lukac (Ed.), Contributed Papers 10th Symposium on Elementary Processes and Chemical Reactions in Low-Temperature Plasma, Stara Lesna, Slovakia, Comenius University, Bratislava, 1994, p. 28.
[11] K. Becker and V. Tarnovsky, Plasma Sources Sci. Technol., 4 (1995) 307.
[12] K. Becker, Comm. At. Mol. Phys., 30 (1994) 261.
[13] S. McGinnis, K. Riehl and P.D. Haaland, Chem. Phys. Lett., 232 (1995) 99.
[14] P. Potzinger and F.W. Lampe, J. Phys. Chem., 74 (1970) 719.
[15] G. Distefano, Inorg. Chem., 9 (1970) 1919.
[16] Eight Peak Index of Mass Spectra, 2nd edn., Mass Spectrometry Data Centre, Aldermaston, 1974; NIST/EPA/NIH Mass Spectral Data Base, Vol. 4.5; Chemical Concepts, P.O. Box 100 202 D-62442 Weinheim, 1994.
[17] M. Ducrepin, J. Dike, R.B. Siegel, V. Tarnovsky and K. Becker, J. Appl. Phys., 73 (1993) 7203.
[18] (a) P. Kurunczi, J.P. Michel, N. Abramzon, K.E. Martus and K. Becker, in K.H. Becker, W.E. Carr and E.E. Kunhardt (Eds.), Contributed papers XXII International Conference on Phenomena in Ionized Gases (ICPIG), Hoboken, NJ, USA, 1995, Stevens Institute of Technology Press, 1995, pp. 2–183.
(b) P. Kurunczi, J.P. Michel, N. Abramzon, A. Koharian,

K.E. Martus and K. Becker, Contr. Plasma Phys., submitted for publication.
[19] R. Basner, M. Schmidt, H. Deutsch, V. Tarnovsky, A. Levin and K. Becker, J. Chem. Phys., 103 (1995) 211.
[20] R. Basner, M. Schmidt and H. Deutsch, Contr. Plasma Phys., 35 (1995) 375.
[21] K. Stephan, H. Helm and T.D. Märk, J. Chem. Phys., 73 (1980) 3763.
[22] D. Margreiter, G. Waldner, H. Deutsch, H.U. Poll, C. Winkler, K. Stephan and T.D. Märk, Int. J. Mass Spectrom. Ion Processes, 100 (1990) 143.
[23] H.U. Poll, C. Winkler, V. Grill, D. Margreiter and T.D. Märk, Int. J. Mass Spectrom. Ion Processes, 112 (1992) 1.
[24] V. Tarnovsky, A. Levin, K. Becker, R. Basner and M. Schmidt, Int. J. Mass Spectrom. Ion Processes, 133 (1994) 175.
[25] SIMION, Version 5.0, Idaho National Engineering Laboratory, EG&E Idaho, Inc., Idaho Falls, ID, 1992.
[26] D. Rapp and P. Englander-Golden, J. Chem. Phys., 43 (1965) 5.
[27] A.F. Hollemann and E. Wiberg, Lehrbuch der Anorganischen Chemie, Walter de Gruyter, Berlin, 1985.
[28] W.H. Press, S.A. Teukolsky, W.T. Vetterling and B.P. Flannery, Numerical Recipes in C. Cambridge University Press, Cambridge, 1992.
[29] H. Deutsch, T.D. Märk, V. Tarnovsky, K. Becker, C. Cornelissen, L. Cespiva and V. Bonacic-Koutecky, Int. J. Mass Spectrom. Ion Processes, 137 (1994) 77.
[30] W.L. Fitch and A.D. Sauter, Anal. Chem., 5 (1983) 832.
[31] H. Deutsch and M. Schmidt, Contrib. Plasma Phys., 25 (1985) 475.
[32] R. Basner, M. Schmidt, H. Deutsch, V. Tarnovksy, A. Levin and K. Becker, J. Chem Phys., 103 (1995) 211.
[33] V. Tarnovsky, A. Levin, H. Deutsch and K. Becker, J. Chem. Phys., 102 (1995) 770.
[34] V. Tarnovsky, A. Levin, H. Deutsch and K. Becker, J. Phys. B, in press.
[35] W.L. Fite and R.T. Brackmann, Phys. Rev., 112 (1958) 1141.
[36] E. Brook, M.F.A. Harrison and A.C.H. Smith, J. Phys. B, 11 (1978) 3115.
[37] R.S. Freund, R.C. Wetzel, R.J. Shul and T.R. Hayes, Phys. Rev. A, 41 (1990) 3575.
[38] M. Gryzinski, Phys. Rev., 138 (1965) 305, 322, 336.
[39] T.A. Daniels, H. Zhu, M.P. Banjaycic and K.T. Leung, Chem. Phys., 159 (1992) 289.